Cardiovasc Intervent Radiol (2008) 31:281–288
DOI 10.1007/s00270-007-9114-6

CLINICAL INVESTIGATION

The Usefulness of Three-Dimensional Angiography with a Flat Panel Detector of Direct Conversion Type in a Transcatheter Arterial Chemoembolization Procedure for Hepatocellular Carcinoma: Initial Experience

Shingo Kakeda · Yukunori Korogi · Yoshihisa Hatakeyama · Norihiro Ohnari · Nobuhiro Oda · Kazuyoshi Nishino · Wataru Miyamoto

Published online: 17 November 2007

Abstract The purpose of this study was to assess the usefulness of a three-dimensional (3D) angiography system using a flat panel detector of direct conversion type in treatments with subsegmental transcatheter arterial chemoembolization (TACE) for hepatocellular carcinomas (HCCs). Thirty-six consecutive patients who underwent hepatic angiography were prospectively examined. First, two radiologists evaluated the degree of visualization of the peripheral branches of the hepatic arteries on 3D digital subtraction angiography (DSA). Then the radiologists evaluated the visualization of tumor staining and feeding arteries in 25 patients (30 HCCs) who underwent subsegmental TACE. The two radiologists who performed the TACE assessed whether the additional information provided by 3D DSA was useful for treatments. In 34 (94.4%) of 36 patients, the subsegmental branches of the hepatic arteries were sufficiently visualized. The feeding arteries of HCCs were sufficiently visualized in 28 (93%) of 30 HCCs, whereas tumor stains were sufficiently visualized in 18 (60%). Maximum intensity projection images were significantly superior to volume recording images for visualization of the tumor staining and feeding arteries of HCCs. In 27 (90%) of 30 HCCs, 3D DSA provided additional useful information for subsegmental TACE. The high-quality 3D DSA with flat panel detector angiography system provided a precise vascular road map, which was useful for performing subsegmental TACE .of HCCs.

Keywords Angiography · Digital subtraction · Digital image · Liver disease · Chemoembolization

S. Kakeda (✉) · Y. Korogi · Y. Hatakeyama · N. Ohnari · N. Oda
Department of Radiology, University of Occupational and Environmental Health School of Medicine, 1-1 Iseigaoka, Yahatanishi-ku, Kitakyushu 807-8555, Japan
e-mail: kakeda@med.uoeh-u.ac.jp

K. Nishino · W. Miyamoto
Technology Research Laboratory, SIMAZU Co., Sohraku-gun, Kyoto 619-0237, Japan

Introduction

Although hepatocellular carcinoma (HCC) is the most common tumor that originates in the liver, hepatic resection frequently is contraindicated because of coexisting cirrhosis [1]. Transcatheter arterial chemoembolization (TACE) is the widely used therapy in patients with HCC who are considered to be unsuitable candidates for surgery, and recent reports have demonstrated survival benefits after TACE [2, 3]. Recent advances in the therapeutic technique of TACE including the development of some types of microcatheter enable us to carry out successful selective and effective treatment to the target with minimum injury to the surrounding liver tissue. Several previous studies have reported that subsegmental TACE may be used effectively as a treatment for small HCC and be considerably superior to the outcome of treatment with conventional TACE [4, 5]. For subsegmental TACE, the interpretation of feeding artery for the treatment of HCC and the understanding of the anatomic relationship of the hepatic artery branches are important factors for successful selective catheterization of the feeding arteries. Although digital subtraction angiography (DSA) has been considered to be the standard criterion for abdominal angiography studies, conventional DSA provides only two-dimensional (2D) projections of the vascular anatomy. Because it is difficult to determine the relationship between multiple

overlapping vessels from 2D projectional images, multiple acquisitions at various angles and catheter location are often necessary to analyze their angioarchitecture precisely. Thus, these multiple acquisitions result in increased radiation exposure to the patient and contrast material. Recently, three-dimensional (3D) angiographic techniques, including 3D DSA and 3D digital angiography, were developed and have been applied clinically to the evaluation of intracranial aneurysms [6–8]. Moreover, some publications have reported the utility of 3D rotational angiography for TACE procedure [9, 10].

3D angiographic techniques with an image intensifier television (II-TV) system have inferior spatial resolution compared with conventional 2D DSA, and did not enable imaging of the entire vascular structures. Recently, a flat panel detector (FPD) of direct conversion type based on amorphous selenium (a-Se) became commercially available for angiography. Compared with the II-TV system, this angiography system using the FPD has several theoretical advantages such as high spatial resolution, wide dynamic range, square field of view, and real-time imaging capabilities with no geometric distortion, and these advantages allow for higher-resolution 3D DSA created from rotational angiography data. The purpose of our prospective study was to assess the usefulness of 3D DSA with this new angiography system in conjunction with 2D DSA for subsegmental TACE in patients with HCC.

Materials and Methods

Case Selection and Classification

From June through October 2004, 36 consecutive patients (25 men, 11 women; age range, 44–82 years; mean age, 69.1 years) who underwent hepatic angiography were prospectively examined. All patients were suspected of having at least one liver tumor on the basis of CT findings. In these patients, the final disease diagnoses were HCC ($n = 33$), cholangiocarcinoma ($n = 1$), metastatic liver tumor ($n = 1$), and hemangioma ($n = 1$). Of the 33 patients with HCC, 19 had histologically proven HCCs, and in the remaining 14 patients, HCC was diagnosed on the basis of a high level of serum α-fetoprotein and the characteristic CT findings. In patients who underwent needle biopsy, typically the biopsy was performed for one lesion. The cholangiocarcinoma and metastatic liver tumor were diagnosed with surgical specimens. A hemangioma was diagnosed on the basis of a characteristic angiographic finding. All patients gave informed consent, and the study was approved by our institutional review board.

Angiography Protocol

All angiography examinations (2D and 3D angiography) were performed using an angiography system with a FPD of direct conversion type on a motorized C-arm (Safire; Shimadzu Corp., Kyoto, Japan). This newly developed detector has a pixel pitch of 150 μm and an array format of 1536 × 1536 pixels, covering a field of view of 23 cm^2. An a-Se film, about 1000 μm thick, is used for the x-ray conversion layer. Using the Seldinger technique, the tip of a 5-Fr catheter was guided from the femoral artery to the descending aorta. First, all patients underwent 2D DSA that included celiac and superior mesenteric angiographic examinations with the use of 24 mL of nonionic contrast material (Iopamiron 300) to evaluate the vascularity of the HCC and the vascular anatomy. Then the 5-Fr catheter was placed in the common hepatic artery, proper hepatic artery, or replaced right hepatic artery if it arose from the superior mesenteric artery, and 10–14 mL of contrast material was manually administered using a 20-mL syringe. After 2D DSA, rotational angiography was performed; the catheter position was the same between 2D DSA and rotational angiography in all patients. 3D data sets were obtained from rotational series consisting of two rotations. This series covers a total angular range of 195 deg around patients, with a first rotation of 60 deg/s to acquire subtraction mask images, and a second rotation of 60 deg/s to acquire opacified images during the administration of contrast material. Data were acquired at 30 frames per second with 1024 × 1024 matrices. The isocenter for the rotational field was the area of interest in the patient's abdomen. The contrast material was automatically administered using a power injector (Autoinjector 120S; Nemoto Kyorindo, Tokyo). In most patients, a delay of 1–3 s and a flow rate of 3–5 mL/s were used, with a total amount of 17–28 mL.

3D Reconstruction Techniques

Image datasets were immediately transferred to a workstation (DAR-5000; 3D-ANGIO option V3.0; Shimadzu Corp.). 3D images were available approximately 3 min after 3D data were transferred to a workstation. MIPs (maximum intensity projections), which were displayed with optimal windows, and VRs (volume renderings), which were displayed with optimal threshold, were reconstructed by a radiologist (Y.H.) who was experienced in angiography. When the radiologists required further information to evaluate the anatomic relationship of the hepatic artery branches, they could independently examine the 3D images on the workstation from desired angles.

Analysis of Overall Image Quality

For evaluation of 3D DSA, two radiologists (S.K., N.O.), who were unaware of clinical findings and did not take part in image manipulation, independently reviewed two different display forms, MIP and VR images, in separate sessions. These 3D images were always evaluated in conjunction with the 2D DSA on hardcopy films. After independent interpretations were performed, the differences in assessments between the two radiologists were resolved by consensus. 3D DSA was displayed on a 19-in. CRT monitor (model RDF192S; Mitsubishi, Tokyo). An intuitive and efficient user interface allows manipulation (e.g., rotation, zoom, electronic scalpel) of these views in real time on this CRT monitor.

Overall image quality was rated according to the degree of visualization of the peripheral branches of the hepatic arteries in field of view using a 4-point scale as follows: 4 = excellent, subsubsegmental branches of the hepatic artery were visualized; 3 = good, all subsegmental branches were clearly visualized; 2 = fair, some subsegmental branches were indistinct; and 1 = poor, no subsegmental branches were visualized [11]. A subsubsegmental branch of the hepatic artery was defined as a peripheral artery that branched from a segmental hepatic artery [11]. Artifacts were evaluated as follows: 4 = no visible artifact, 3 = minimal artifact that did not interfere with diagnostic quality, 2 = moderate artifact sufficient to interfere with diagnostic quality, and 1 = heavy artifact resulting in nondiagnostic study. When an artifact was presented, radiologists were asked to indicate the locations and characteristics of artifacts such as patient's motion artifact, cardiac motion artifact, and respiratory motion artifact.

Analysis in Subsegmental TACE

Of 33 patients with HCCs, subsegmental TACE was not performed in 4 patients because of large HCCs (n = 2) or multiple HCCs (n = 2). In 3 (4 HCCs) of the remaining 29 patients (36 HCCs), selective catheterization distal to the subsegmental artery failed technically or was anatomically impossible, thus the success rate of subsegmental catheterization was 89% (32 of 36 HCCs). One (2 HCCs) of 26 patients (32 HCCs) was excluded from the evaluation because the field of view did not cover the tumor staining on 3D DSA. Therefore, 30 HCCs in 25 patients were included in this evaluation; two radiologists evaluated the visualization of the tumor staining and feeding arteries for the 30 HCCs (nodule size range, 5–40 mm in diameter; mean, 18.0 mm; median, 15.0 mm). Three-phase (arterial, portal, and delayed phases) spiral CT obtained before hepatic DSA detected all 30 HCCs; 29 of 30 HCCs were detected in the arterial phase, which is better than in the portal phase (n = 17) and the delayed phase (n = 20). Lesions and diameters of the tumors were determined with 2D DSA. Three of 30 HCCs were located in segment S3, 5 in S4, 6 in S5, 5 in S6, 2 in S7, and 9 in S8.

The following scale was used to evaluate tumor staining: 5 = excellent (tumor staining depicted with close to the same quality as with 2D DSA); 4=good (tumor staining clearly visualized but image quality somewhat reduced compared with that with 2D DSA); 3 = adequate (blurred visualization of tumor staining but providing sufficient useful information for TACE); 2 = insufficient visualization; and 1 = not visible. Feeding artery for the treatment of HCC was evaluated as follows: 5 = excellent (vessel segment clearly visualized and vessel-tissue contrast high); 4 = good (satisfactory visualization but vessel-tissue contrast somewhat reduced); 3 = adequate (visualization of vessel segment still sufficient); 2 = insufficient visualization; and 1 = not visible. When tumor staining and the feeding artery of HCC were evaluated as 2 or 1 (insufficient visualization or not visible), the readers were asked to indicate possible reasons for nonvisualization, such as patient motion, cardiac motion artifact, respiratory motion artifact, or poor contrast enhancement.

In addition, two radiologists who performed or assisted with subsegmental TACE were questioned as to whether the additional information provided by 3D angiography was useful for treatment. The answers of these radiologists for each HCC were scored as follows: grade 3, 3D DSA provided very useful information that was helpful for the TACE approach, and interventional radiologists could perform selective catheterization of the feeding artery without a further hepatic angiography session after the 3D DSA session; grade 2, 3D DSA provided sufficient information that was helpful for the TACE approach and could reduce further hepatic angiography sessions after the 3D DSA session; grade 1, 3D DSA provided further information that was not helpful for TACE; or grade 0, 3D DSA provided no further information. The judgments were obtained by consensus.

Statistical Analysis

All statistical analyses were performed with a statistical software package (StatView 5.0; SAS Institute, Cary, NC). For scores of image quality, all results are expressed as the mean ± standard error of the mean for each reconstruction technique (MIP and VR image). Analysis of Wilcoxon signed rank test was performed on the results to assess the statistical significance of the different scores assigned to MIP and VR images. A p value of <0.05 was considered to indicate a statistically significant difference. To evaluate

the level of interobserver agreement on scores of image quality, a Kendall *W* test was performed. Kendall *W* coefficients between 0.5 and 0.8 were considered to indicate good agreement, and coefficients >0.8 were considered to indicate excellent agreement.

Results

Conventional 2D DSA and rotational angiography were successfully performed in all 36 patients without any complications, and a diagnostic image was obtained in all patients. Rotational angiography was performed with catheterization at the common hepatic artery ($n = 24$), the proper hepatic artery ($n = 9$), or the replaced right hepatic artery arising from the superior mesenteric artery ($n = 3$).

The overall image quality of MIP images was scored to be excellent in 29 (80.6%) of 36 patients, good in 5 (13.9%), and fair in 2 (5.6%), while the overall image quality of VR images was excellent in 15 (41.7%), good in 18 (50%), and fair in 3 (8.3%) (Table 1). The mean rating scores for the overall image quality were 3.75 ± 0.55 (mean $\pm$ SD) for MIP images and 3.33 ± 0.63 for VR images ($p < 0.001$; Wilcoxon signed rank test). In 34 (94.4%) patients the subsegmental branches of the hepatic artery were sufficiently visualized on MIP images. None of the examinations revealed artifacts that resulted in a non-diagnostic study. Moderate artifacts due to identifiable cardiac motion, which interfered with the image quality in visualization of the subsegmental hepatic artery branches, were observed on the left lateral lobe in two (5.6%) patients each for both MIP and VR images (Fig. 1). There were minimal artifacts, associated with misregistration due to respiratory motion, in 10 (27.8%) for MIP and 3 (8.3%) for VR images. All these artifacts were present on the diaphragmatic surface (Fig. 2).

The results on visualization of tumor staining and feeding artery are summarized in Table 2. Sufficient visualization of tumor staining (score, 5–3) was obtained in 18 (60.0%) of 30 HCCs for MIP images and in 11 (37.6%) for VR images; MIP images were significantly superior to VR images (mean rating score, 2.80 ± 1.35 vs.

Fig. 1 Images in a 71-year-old woman with hepatocellular carcinoma. MIP image from the inferior and right anterior oblique view obtained with contrast material injection in the selective common hepatic artery. An artifact due to identifiable cardiac motion interferes with the diagnostic quality of the hepatic artery in the left lateral lobe (arrows)

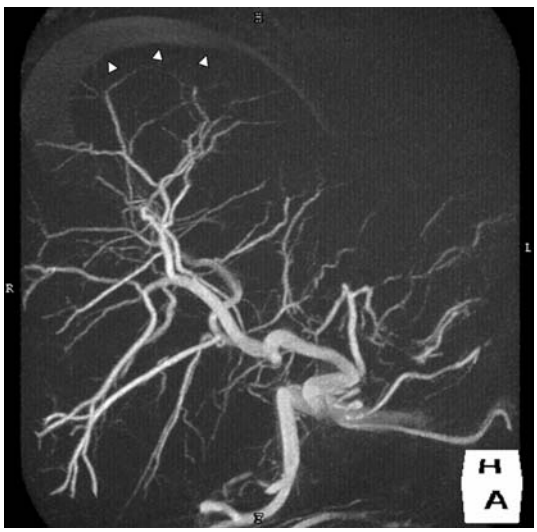

Fig. 2 Images in a 56-year-old woman with cholangiocarcinoma. MIP image shows a respiratory misregistration artifact associated with the subtraction technique on the diaphragmatic surface (arrowheads)

Table 1 Evaluation of 3D DSA with regard to visualization of the peripheral branches of the hepatic artery

	Score for overall image quality				Mean $\pm$ SD[a]	*p* value[b]
	4	3	2	1		
MIP ($n = 36$)	29 (80.6%)	5 (13.9%)	2 (5.6%)	0 (0.0%)	3.75 ± 0.55	
VR ($n = 36$)	15 (41.7%)	18 (50.0%)	3 (8.3%)	0 (0.0%)	3.33 ± 0.63	<0.001

Note. Data are the number of patients

[a] Data are mean $\pm$ SD of scores for overall image quality evaluated using a 4-point scale (4 = excellent, 3 = good, 2 = fair, 1 = poor)

[b] Wilcoxon signed rank test

Table 2 Evaluation of 3D DSA with regard to visualization of tumor staining and feeding artery

		Score for image quality					Mean ± SD[a]	*p* value[b]
		5	4	3	2	1		
Tumor staining (n = 30)	MIP	4 (13.3%)	5 (16.7%)	9 (30.0%)	5 (16.7%)	7 (23.3%)	2.80 ± 1.35	<0.001
	VR	0 (0.0%)	3 (10.0%)	8 (26.7%)	5 (16.7%)	14 (46.7%)	2.00 ± 1.08	
Feeding artery (n = 30)	MIP	21 (70.0%)	6 (20.0%)	1 (3.3%)	1 (3.3%)	1 (3.3%)	3.50 ± 0.97	<0.001
	VR	9 (30.0%)	12 (40.0%)	6 (20.0%)	1 (3.3%)	2 (6.7%)	2.83 ± 1.12	

Note. Data are the number of patients

[a] Data are mean ± SD scores for image quality evaluated using a 5-point scale (5 = excellent, 4 = more than adequate, 3 = adequate, 2 = insufficient visualization, 1 = not visible)

[b] Wilcoxon signed rank test

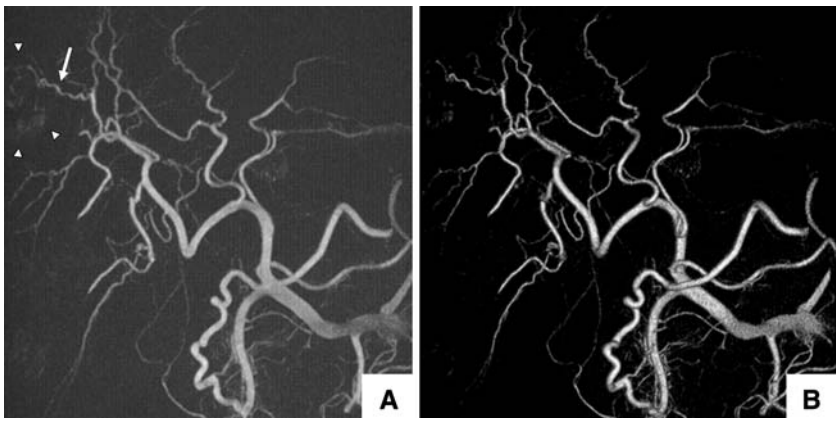

Fig. 3 Images in a 71-year-old man with hepatocellular carcinoma. (**A**) MIP image and (**B**) VR image from the left oblique view obtained with contrast material injection in the selective common hepatic artery. MIP image sufficiently reveals the tumor stain (arrowheads) and the feeding artery (arrow); however, the tumor stain was insufficiently visualized on VR image

2.00 ± 1.08; $p < 0.001$) (Fig. 3). The reason for the poor or absent visualization of tumor staining was insufficient contrast enhancement of the tumors in all (12 for MIP and 19 for VR images). Sufficient visualization of feeding arteries (score, 5–3) was obtained in 28 (93.3%) of 30 HCCs on MIP images; MIP images were significantly superior to VR images (mean rating score, 3.50 ± 0.97 vs. 2.83 ± 1.12; $p < 0.001$). Visualization was scored as excellent in 21 (70.0%) for MIP images and in 9 (30.0%) for VR images. The reasons for poor or absent visualization of feeding arteries were insufficient contrast of the vessels in all (two HCCs for MIP and three HCCs for VR images).

The additional information for the TACE approach provided by 3D DSA was ranked grade 3 in 10 (33.3%) of 30 HCCs (Figs. 4 and 5), grade 2 in 17 (56.7%), and grade 1 in 3 (10.0%), and no HCC was ranked grade 0 (no further information).

Interobserver Agreement

For evaluation of 3D DSA, interobserver agreement between the two radiologists in rating image quality parameters were good or excellent for both MIP and VR images, respectively, with Kendall W values (τ) of 0.92 and 0.84 for rating of overall image quality, 0.99 and 0.94 for rating of visualization of tumor staining, and 0.80 and 0.83 for rating of visualization of feeding artery.

Discussion

Currently, two types of FPD architecture have been proposed, one being an indirect detection type and the other a direct detection type. In the indirect detection type, absorbed x-ray photons are converted to photons of visible light in a scintillator layer (e.g, amorphous silicon or cesium iodide), and the photons are then detected by a two-dimensional photodiode array. In contrast, in the direct detection type, absorbed x-ray photons are directly converted to electron hole pairs in a conversion layer (e.g., amorphous selenium) and then collected as electric charges on storage capacitors [12–14]. The direct detection type has superior spatial resolution to the indirect detection type because of its simple conversion process 15]. There are several studies in the literature which investigate the use of FPD of direct conversion type in radiography [16–19]; however, few studies dealing with an angiography system using a FPD of the direct conversion type have been done.

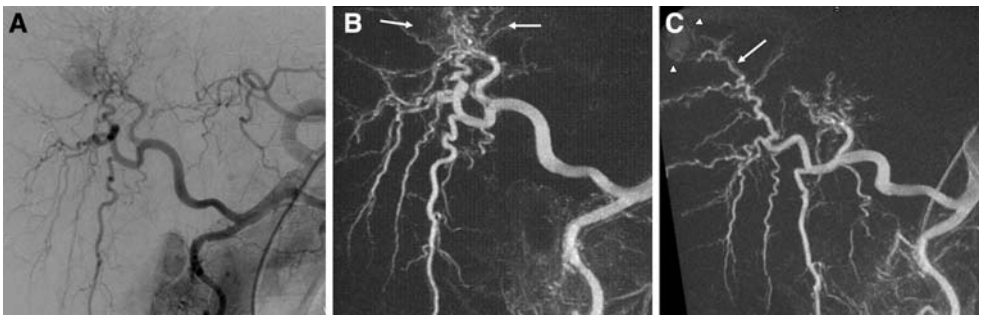

Fig. 4 Images in a 69-year-old woman with hepatocellular carcinoma. Anteroposterior selective common hepatic angiograms, (**A**) 2D DSA and (**B**) MIP image, show tumor staining in the liver. However, the relationship between the tumor staining and the feeding artery (arrows) is unclear. (**C**) The superior and right anterior oblique MIP image clearly reveals the relationship between the tumor staining (arrowheads) and the feeding artery (arrow)

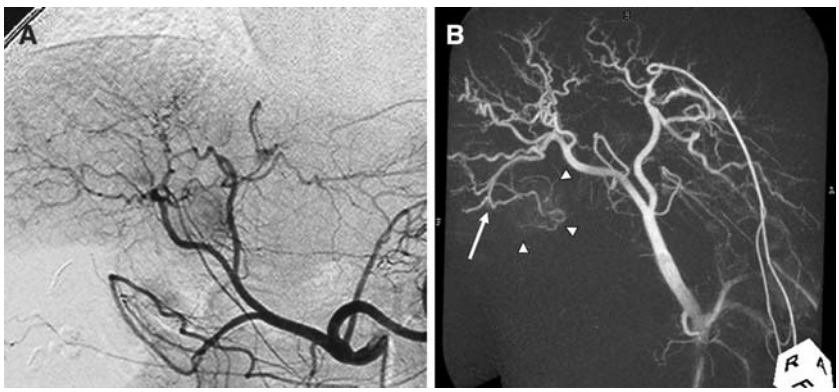

Fig. 5 Images in a 57-year-old woman with hepatocellular carcinoma. (**A**) Anteroposterior celiac angiogram (2D DSA) shows the tumor staining and feeding artery. However, the relationship between the feeding artery for the treatment of HCC and the other hepatic artery branches are unclear. (**B**) MIP image from the inferior and right anterior oblique view obtained with contrast material injection in the selective common hepatic artery clearly reveals the tumor stain (arrowheads) and the anatomic relationship between the feeding artery (arrow) and the other hepatic artery branches. For TACE, the MIP image provided the guidance for successful catheterization by visualizing the origin of hepatic branch vessels

Our study demonstrated that the subsegmental branches of the hepatic artery were sufficiently visualized in 34 (94.4%) patients on MIP images of 3D DSA. The theoretical advantages with the FPD such as the high spatial resolution and wide dynamic range may allow precise visualization of small and peripheral vessels on 3D DSA. Modulation transfer function (MTF) is generally accepted as the most important parameter of spatial resolution for characterizing the performance of a detector system. Although measurements of physical imaging characteristics cannot be directly related to expected observer performance in a diagnostic setting, there is general agreement that a higher MTF is indicative of superior image quality. The FPD used in this study shows a high MTF in previous experimental testing [20]. Another major advantage of the FPD is the wide dynamic range of the detector. The dynamic range of our FPD system is 1:10,000 according to the manufacturers' specifications. The wide dynamic range may explain the better visualization of the peripheral small vessels in the right subphrenic location where large differences in x-ray absorption exist between the liver and lung regions. Another reason for the high image quality in depicting peripheral vessels may be that the FPD has an imaging capability with no geometric distortion. This characteristic allows excellent uniformity of response and resolution across its area.

In our study, although 2D DSA demonstrated tumor staining for all 30 HCCs, MIP images of 3D DSA visualized tumor staining in only 18 (60.0%) of 30 lesions. There are several possible reasons for this result. First, the contrast resolution and signal-to-noise performance of 3D DSA may not be sufficient for visualization of relatively faint staining of tumors in comparison with 2D DSA. Second, since we arbitrarily determined the volume of contrast material and the delay time from the start of the injection, insufficient tumor staining may be related to an insufficient time for a substantial amount of contrast material to reach the tumor during. Further evaluation is necessary to determine the optimal timing of rotational angiography for better visualization of tumor staining.

Third, complicated blood supplies of HCCs in underlying cirrhosis from both the portal vein and the hepatic artery may affect the visualization of tumor staining during rotational angiography [21–23].

This study was not intended to evaluate the additional diagnostic value of 3D DSA images in the depiction of HCCs but, rather, to assess the additional value of 3D DSA images for the subsegmental TACE procedure over 2D DSA alone. 3D DSA provided guidance of successful catheterization by viewing the origin of branch vessels. It is important for endovascular catheterization to find a 2D view that clearly depicts the anatomic relationship of the hepatic artery branches. In most patients, we found some optimal views using 3D DSA and reduced the multiple oblique acquisitions that are usually needed with 2D DSA. In addition, it is important to note that, even in patients without tumor staining on 3D DSA, 3D DSA provided additional useful information for interventional radiologists by combined inspection with 2D DSA and/or preinterventional CT studies.

Reduction of multiple oblique acquisitions with the use of 3D DSA also leads to a reduction in radiation exposure to patients. Radiation injuries are typically divided into two types of effects, deterministic and stochastic. Deterministic effects are those associated with a minimum threshold dose below which the effect is not seen. Examples of deterministic effects include early transient erythema, temporary epilation (hair loss), and cataracts. Recently, it has been reported that the radiation dose for TACE could lead to local transient erythema in many patients [24]. Further study is required to determine how much reduction of the radiation dose can be obtained with active use of 3D DSA in each patient who undergoes TACE. We reported that our FPD system allowed a significant reduction of patient exposure in comparison with the II-TV system during 2D DSA, maintaining superior spatial resolution [25]. Therefore, our system may have an additive positive effect of the FPD itself and 3D DSA for the control of radiation exposure during interventions.

In this study, two postprocessing algorithms, MIP and VR images, of 3D DSA were compared, and MIP image was superior to VR image for visualization of the tumor staining and feeding artery. The MIP algorithm selects only the voxel with the highest attenuation along a ray projected through the data set, and this characteristic of reconstruction algorithm seems to allow the depiction of low-contrast objects, such as tumor staining and feeding artery down to the subsegmental level. Unlike the MIP image, the VR image is a weighted sum of data from all voxels along lines projected through the data set. Therefore the VR image maintains the original anatomic spatial relationships of the 3D angiographic data set. Although VR image has been reported to be superior to MIP image in demonstrating the interpretation of vascular interrelationships [26, 27], we believe that the MIP image is enough for understanding the anatomic relationship of the hepatic artery branches when the MIP image was analyzed from desired views in real time on the workstation.

Another purpose of our study was to assess the degree of degradation in image quality caused by artifacts, such as patient motion artifact, cardiac motion artifact, and respiratory motion artifact. For CT angiography, respiratory motion artifact was considered the main cause of inadequate visualization of the hepatic arterial anatomy [28]. In this study, artifacts due to respiratory motion did not interfere with diagnostic quality, probably because of the short acquisition time for the 3D data, which is approximately 3 s in a single breath hold. Although cardiac motion artifacts were seen on the left lateral segment in two patients, they did not interfere with the diagnostic quality of the feeding artery and tumor staining because there were no tumors in the left lateral segment in these patients. It will be necessary to investigate the effects of cardiac motion artifacts on HCCs in the left lateral segment.

A major limitation of the system used in this study is the small field of view (9 in. [22.9 cm^2]), which may not be large enough for examination of the abdomen. Recently, however, a large-area FPD (41 $\times$ 41 cm^2) for angiography has been reported in the laboratory environment [29, and it will probably be used clinically in the near-future.

In conclusion, our FPD angiography system based on a-Se can create high-quality 3D DSA, which can provide a precise vascular roadmap to determine the feeding arteries of HCCs during subsegmental TACE. This information is expected to help reduce the dose of radiation and contrast material by facilitating attempts at selective catheterization of the feeding arteries of hepatic tumors.

References

1. Zamann SN, Johnson PJ, Williams R (1990) Silent cirrhosis in patients with hepatocellular carcinoma. Cancer 65:1607–1610
2. Yuen MF, Chan AO, Wong BC, et al. (2003) Transarterial chemoembolization for inoperable, early stage hepatocellular carcinoma in patients with Child-Pugh grade A and B: results of a comparative study in 96 Chinese patients. Am J Gastroenterol 98:1181–1185
3. O'Suilleabhain CB, Poon RT, Yong JL, Ooi GC, Tso WK, Fan ST (2003) Factors predictive of 5-year survival after transarterial chemoembolization for inoperable hepatocellular carcinoma. Br J Surg 90:325–331
4. Matsui O, Kadoya M, Yoshikawa J, et al. (1993) Small hepatocellular carcinoma: treatment with subsegmental transcatheter arterial embolization. Radiology 188:79–83
5. Itsubo M, Koike K, Tsuno S, et al. (2002) Subsegmental transcatheter arterial embolization for small hepatocellular carcinoma. Hepatogastroenterology 49:735–739
6. Anxionnat R, Bracard S, Ducrocq X, et al. (2001) Intracranial aneurysms: clinical value of 3D digital subtraction angiography

in the therapeutic decision and endovascular treatment. Radiology 218:799–808
7. Tanoue S, Kiyosue H, Kenai H, Nakamura T, Yamashita M, Mori H (2000) Three-dimensional reconstructed images after rotational angiography in the evaluation of intracranial aneurysm: surgical correlation. Neurosurgery 47:866–871
8. Hirai T, Korogi Y, Suginohara K, et al. (2003) Clinical usefulness of unsubtracted 3D digital angiography compared with rotational digital angiography in the pretreatment evaluation of intracranial aneurysms. Am J Neuroradiol 24:1067–1074
9. Tanigawa N, Komemushi A, Kojima H, Kariya S, Sawada S (2004) Three-dimensional angiography using rotational digital subtraction angiography: usefulness in transarterial embolization of hepatic tumors. Acta Radiol 45:602–607
10. Liapi E, Hong K, Georgiades CS, Geschwind JF (2005) Three-dimensional rotational angiography: introduction of an adjunctive tool for successful transarterial chemoembolization. J Vasc Interv Radiol 16:1241–1245
11. Tanikake M, Shimizu T, Narabayashi I, et al. (2003) Three-dimensional CT angiography of the hepatic artery: use of multi-detector row helical CT and a contrast agent. Radiology 227:883–889
12. Rowlands JA, Hunter DM, Araj N (1991) X-ray imaging using amorphous selenium: a photoinduced discharge readout method for digital mammography. Med Phys 18:421–431
13. Chotas HG, Dobbins JT, Rabin CE (1999) Principles of digital radiography with large-area, electronically readable detectors: a review of the basics. Radiology 210:595–599
14. Zhao W, Ji WG, Debrie A, Rowlands JA (2003) Imaging performance of amorphous selenium based flat-panel detectors for digital mammography: characterization of a small area prototype detector. Med Phys 30:254–263
15. Tsukamoto A, Yamada S, Tomisaki T, et al. (1999) Development and evaluation of a large-area selenium-based flat panel detector for real-time radiography and fluoroscopy. Proc SPIE 3659:14–23
16. Woodard PK, Slone RM, Gierada DS, Reiker GG, Pilgram TK, Jost RG. (1997) Chest radiography: depiction of normal anatomy and pathologic structures with selenium-based digital radiography versus conventional screen-film radiography. Radiology 203:197–201
17. Woodard PK, Slone RM, Sagel SS, et al. (1998) Detection of CT-proved pulmonary nodules: comparison of selenium-based digital and conventional screen-film chest radiographs. Radiology 209:705–709
18. Neitzel U, Maack I, Günther-Kohfahl S (1994) Image quality of a digital chest radiography system based on a selenium detector. Med Phys 21:509–516
19. Kim TS, Im JG, Goo JM, et al. (2002) Detection of pulmonary edema in pigs: storage phosphor versus amorphous selenium-based flat-panel-detector radiography. Radiology 223:695–701
20. Adachi S, Hori N, Sato K, et al. (2000) Experimental evaluation of a-Se and CdTe flat-panel x-ray detectors for digital radiography and fluoroscopy. Proc SPIE 3977:38–47
21. Jang HJ, Lim JH, Lee SJ, Park CK, Park HS, Do YS (2000) Hepatocellular carcinoma: are combined CT during arterial portography and CT hepatic arteriography in addition to triple-phase helical CT all necessary for preoperative evaluation? Radiology 215:373–380
22. Peterson MS, Baron RL, Dodd GD III, et al. (1992) Hepatic parenchymal perfusion defects detected with CTAP: imaging-pathologic correlation. Radiology 185:149–155
23. Oliver III JH, Baron RL, Dodd III GD, Peterson MS, Carr BI (1995) Does advanced cirrhosis with portosystemic shunting affect the value of CT arterial portography in the evaluation of the liver? AJR 164:333–337
24. Hidajat N, Wust P, Felix R, Schroder RJ (2006) Radiation exposure to patient and staff in hepatic chemoembolization: risk estimation of cancer and deterministic effects. Cardiovasc Interv Radiol 29:791–796
25. Hatakeyama Y, Kakeda S, Korogi Y, et al. (2006) Intracranial 2D and 3D DSA with flat panel detector of the direct conversion type: initial experience. Eur Radiol 16:2594–2602
26. Johnson PT, Heath DG, Kuszyk BS, Fishman EK (1996) CT angiography with volume rendering: advantages and applications in splanchnic vascular imaging. Radiology 200:564–568
27. Sugahara T, Korogi Y, Nakashima K, Hamatake S, Honda S, Takahashi M (2002) Comparison of 2D and 3D digital subtraction angiography in evaluation of intracranial aneurysms. Am J Neuroradiol 23:1545–1552
28. Lee SS, Kim TK, Byun JH, et al. (2003) Hepatic arteries in potential donors for living related liver transplantation: evaluation with multi-detector row CT angiography. Radiology 227:391–399
29. Granfors PR, Aufrichtig R (2000) Performance of a 41 × 41-cm^2 amorphous silicon flat panel x-ray detector for radiographic imaging applications. Med Phys 27:1324–1331